Water Splitting

DOI: 10.1002/ange.201406800

The Role of Surface States in the Oxygen Evolution Reaction on Hematite**

Beniamino Iandolo and Anders Hellman*

Abstract: *Hematite (α-Fe_2O_3) is an extensively investigated semiconductor for photoelectrochemical (PEC) water splitting. The nature and role of surface states on the oxygen evolution reaction (OER) remain however elusive. First-principles calculations were used to investigate surface states on hematite under photoelectrochemical conditions. The density of states for two relevant hematite terminations was calculated, and in both cases the presence and the role of surface states was rationalized. Calculations also predicted a Nerstian dependence on the OER onset potential on pH, which was to a very good extent confirmed by PEC measurements on hematite model photoanodes. Impedance spectroscopy characterization confirmed that the OER takes place via the same surface states irrespective of pH. These results provide a framework for a deeper understanding of the OER when it takes place via surface states.*

Sunlight-driven photoelectrochemical (PEC) water splitting carries the promise of an efficient, sustainable method for harvesting solar energy and storing it in chemical bonds in form of fuels.[1–3] To make PEC water splitting economically competitive, we need photoelectrodes that are inexpensive, stable against corrosion, as well as efficient in converting solar energy into chemical energy.[4] The latter requirement translates into: broad absorption of sunlight, high yield of charge carriers delivered to the appropriate semiconductor/electrolyte interface, and high catalytic activity for both hydrogen and oxygen evolution reactions (HER and OER, respectively). Since no photoelectrode has been found so far to satisfy all these requirements simultaneously,[5] research has focused on identifying materials that efficiently address some of the processes taking place in a PEC cell. In this context, hematite (α-Fe_2O_3) has attracted great interest as photoanode for the OER,[6–14] being an inexpensive semiconductor, stable in electrolytic environment of pH higher than 3,[15] and capable of absorbing a significant amount of visible light thanks to its bandgap energy of around 2 eV.[16] The microscopic mechanism of the OER on hematite is currently the object of intense investigation. It is generally agreed that surface states play an important role in determining the OER efficiency.[9,17] The latter is usually limited by recombination at these surface states. However, the chemical identity and role of the states are not fully understood.[18] In particular, it is not clear whether they are intermediates in the OER, or instead participate in parasitic reactions. Herein, we used a unique combination of first-principles calculations and PEC characterization to investigate the role of surface states on the OER on hematite. Density functional theory (DFT) calculations were employed to resolve the density of states (DOS) for OH-terminated and O-terminated hematite surfaces. The OH-terminated surface is associated with occupied surface states extending over a broad range of energies in the bandgap, while the O-terminated surface is characterized by occupied surface states close to the top of the valence band. The electrochemical potential at which the O-terminated surface becomes more stable corresponds to the predicted onset potential of the OER, V_{onset}. The OER then takes place via the surface states, the energy of which is just above the top of the valence band. Moreover, V_{onset} is predicted to decrease linearly with increasing pH, following the Nernst equation. Such dependence of V_{onset} on pH is not expected if only the position of the valence band edge in hematite and the OER potential are considered, which both shift according to the same Nerstian dependence[19] (although a somewhat beneficial effect of increasing the pH from neutral to basic has been reported in terms of cathodic shift of V_{onset}).[20] These predictions are confirmed to a large extent by PEC characterization of model photoanodes based on hematite thin films. Impedance spectroscopy confirmed the presence of surface states that are discharged when the OER is initiated, and V_{onset} shifted linearly towards more cathodic potentials with a slope of 49 mV per pH unit.

DFT calculations were performed as implemented in VASP,[21–23] and the computational electrochemical framework of Rossmeisl et al. was adapted[24,25] (see Experimental Section for details). Figure 1 shows the calculated DOS for bulk hematite, OH-terminated and O-terminated hematite (top, middle, and bottom panel, respectively). To facilitate the comparison between the three cases, the edges of the conduction band in each case are aligned. With the present theoretical approach the band gap in bulk hematite is 1.8 eV, which is in good agreement with the optical bandgap values of 1.9–2.2 eV reported in various studies, depending on the utilized fabrication route. The atom-resolved DOS indicates that the valence band is formed by p-band contribution from O atoms, whereas the conduction band has mostly a Fe d-band character, in excellent agreement with previous results.[26] The OH-terminated surface is of particular interest in the context of (photo)electrochemistry, since both calcu-

[*] B. Iandolo, Dr. A. Hellman
Applied Physics Department, Chalmers University of Technology
Fysikgränd 3, SE-41296 Göteborg (Sweden)
E-mail: iandolo@chalmers.se
ahell@chalmers.se

[**] Support from the Swedish Research Council, Formas (project numbers 219-2011-959 and 229-2009-772), and the Chalmers Area of Advance Material and Energy is gratefully acknowledged.

Supporting information for this article is available on the WWW under http://dx.doi.org/10.1002/anie.201406800.

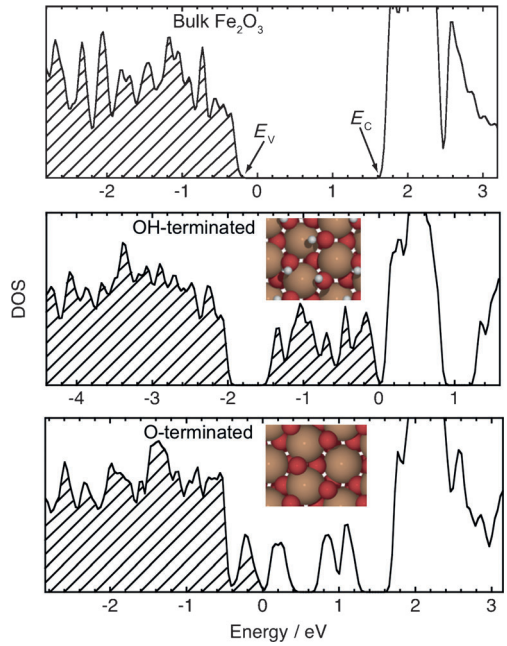

Figure 1. The calculated density of states for bulk hematite (top panel), OH- covered hematite (middle panel), and O- covered hematite (bottom panel). The area under the occupied states is shaded. The insets in the middle and bottom panel show the OH-terminated and O-terminated hematite surface, respectively. H white, O red, Fe brown.

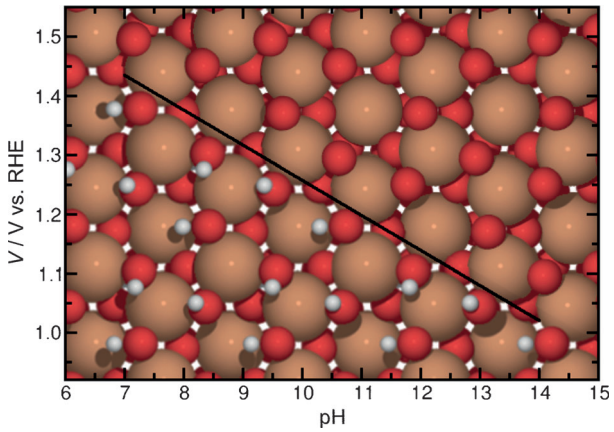

Figure 2. The calculated electrochemical threshold potential between the regions of stability for the OH- and O-terminated hematite surfaces as function of pH. H white, O red, Fe brown.

lations and experiments indicate that hematite undergoes spontaneous surface hydroxylation when exposed to aqueous electrolytes.[9,27] It is clear that the OH termination introduces occupied mid-gap surface states in a broad energy range extending about 1.5 eV from the bottom of the conduction band. Surface states are also present in the O-terminated surface (corresponding to the regime in which the OER takes place), although the DOS is considerably different. In particular, only the DOS peak closest to the top of the valence band is occupied. Combining the information from calculated DOS with the energetics of the hematite/electrolyte junction, the role of surface states on the OER can be rationalized in the following way. In the case of OH-terminated surface, any beneficial effect on the OER of the photon induced additional driving force is negated by the presence of the filled surface states extending over most of the bandgap, which causes a pinning of the quasi-Fermi energy for holes $E_{F,p}$. This results in surface recombination without OER. For potentials more anodic than the threshold potential corresponding to the transition to the O-terminated surface, the surface states are empty until an energy of approximately 0.4 eV higher than the top of the valence band. As a consequence, $E_{F,p}$ is no longer pinned, and holes have enough energy to contribute to the OER by transferring from the states just above the top of the valence band. Increasing the potential even further empties the surface states completely, thus allowing holes from the valence band to take part in the OER by direct transfer. The presence of these two pathways is expected to manifest itself in a difference in the response of the system to impedance spectroscopy performed under appropriate potentials. Figure 2 shows the electrochemical potential threshold at which the OH-terminated surface becomes less stable as compared to the O-terminated one, which leads to the start of the OER, as function of pH. We stress that the electrochemical potential scale used here is the reversible hydrogen electrode (RHE), against which both the OER potential and the top of the valence band in hematite have a fixed value. The calculated threshold potential follows a linear behavior according to the Nernst equation (that is, a slope of 59 mV per pH unit), as it reflects the decrease in free energy of the OH-terminated surface. To test the predictions of the calculations presented above, detailed PEC characterization, namely cyclic voltammetry, open circuit measurements, and electrochemical impedance spectroscopy (EIS), was performed on model photoanodes consisting of hematite films deposited on top of indium tin oxide (ITO), in a standard three-electrode configuration (see Experimental Section and Supporting Information for more details). These films are polycrystalline[28] and with a relatively flat surface (Supporting Information, Figure S2 and S3), which makes the interpretation of EIS results less complicated than in the case of nanostructured electrodes. For the sake of clarity, we show here results from measurements performed on a single photoanode. However, several photoanodes were characterized showing the same quantitative trends in PEC properties. Figure 3a shows current–voltage (or J–V) plots for a hematite photoanode in contact with electrolytes of pH varying from 6.9 to 13.6, under AM 1.5 solar simulated illumination. Indeed, a clear cathodic shift of V_{onset} is observed for increasing pH, with the most negative V_{onset} found for the most basic electrolyte (consisting of 0.5 M Na_2SO_4 + 1 M KOH). We also note that the maximum photocurrent measured before the onset of the OER in the dark is very similar (around 0.2 mA cm^{-2}) for all the electrolytes used.

The PEC properties of the samples were further investigated by EIS, which is an excellent method to obtain information about processes taking place at the surface of and in the photoanode material, provided an appropriate equivalent circuit (EC) is employed to fit the impedance spectra acquired.[29] Thanks to EIS, among other techniques, the role

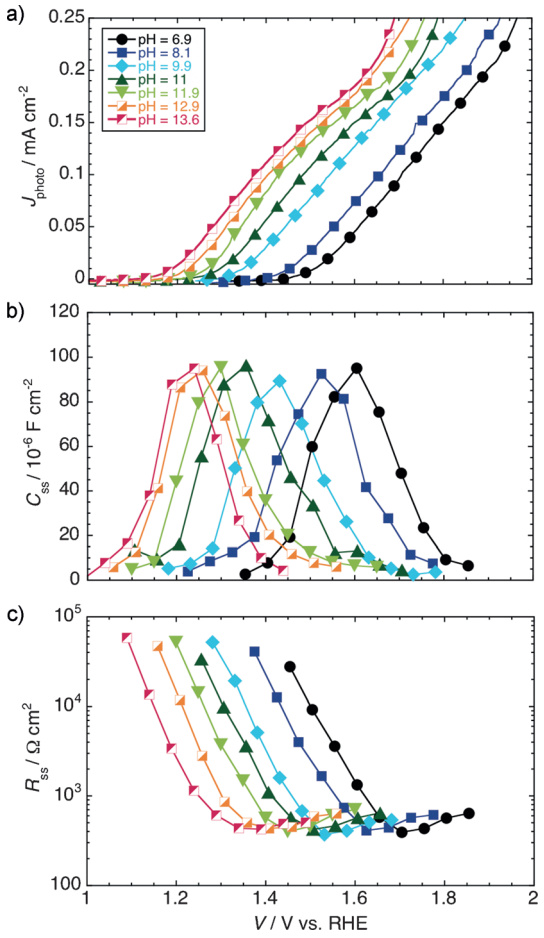

Figure 3. PEC measurements on a hematite photoanode immersed in electrolytes with varying pH, under AM 1.5 solar simulated illumination. a) *J*–*V* plots showing a cathodic shift of V_{onset} for increasing pH, even when using a reference scale for the electrochemical potential, the RHE, against which both the OER potential and the top of the valence band in hematite have a fixed value. b) Surface-state capacitance C_{SS} extracted from fitting of Nyquist plots obtained from EIS measurements. The peak in C_{SS} (typically found in system where the OER takes place via surface states) is found to shift cathodically with increasing pH, just as V_{onset}. c) Hematite/electrolyte charge-transfer resistance R_{SS}, also from fitting of the Nyquist plots. Like C_{SS}, R_{SS} is found to have very similar behavior for varying pH, showing a minimum that shifts towards more cathodic potentials with increasing pH.

of surface states in photon-driven OER on hematite has been thoroughly investigated.[20,30,31] Representative Nyquist plots from EIS characterization under illumination for one of the electrolytes used here are shown in the Supporting Information, Figure S5. The presence of two semicircles in the plots can be seen, one having an almost constant radius for increasing DC bias, and one whose radius decreases considerably until it basically disappears for the highest bias shown. The EC employed to fit the Nyquist plots is described in the Supporting Information, Figure S6, and has been discussed in detail.[27] In brief, its components are: the series resistance R_S between ITO and hematite, the space-charge layer capacitance C_{bulk}, the bulk charge trapping resistance R_{trap}, the capacitance associated with surface states C_{SS}, and the charge transfer resistance across the hematite/electrolyte junction, R_{SS}. The presence of two capacitances in the system is behind the two semicircles in the Nyquist plots. Figure 3b and c illustrate the behavior of C_{SS} and of R_{SS}. Both show very similar trends, with a maximum and a dip respectively, for all electrolytes. The potential for which C_{SS} shows a maximum shows excellent agreement with the OER V_{onset}, after which it decreases until it is back to negligible values for highly anodic potentials, that is, 0.3-0-4 V higher than V_{onset}. This is an experimental confirmation that that the OER proceeds via surface states and via direct transfer from the valence band for moderately and highly anodic potentials, respectively.

Figure 4 shows the results from a more quantitative analysis of the shift of V_{onset} described above. Several

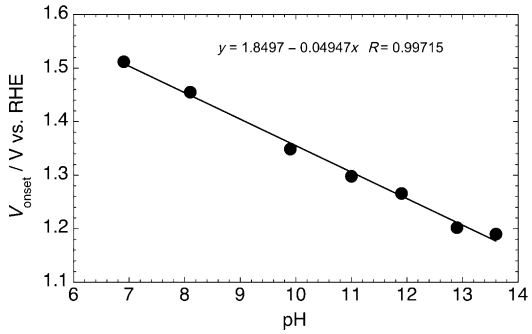

Figure 4. The onset potential V_{onset} for the OER under solar simulated illumination, as a function of the pH of the electrolyte. A linear cathodic shift of V_{onset} is observed upon increasing the pH from 6.9 to 13.6, with a linear coefficient of 49 mV per pH unit.

approaches have been used to determine the values of V_{onset} from a *J*–*V* plot.[32–34] Following the criterion described in a previous work, we defined V_{onset} as the potential value at which the photocurrent density exceeds 10^{-5} A cm^{-2}. V_{onset} is then found to shift of 320 mV, from the most anodic value of 1.51 V vs. RHE for a pH of 6.9, to the most cathodic value of 1.19 V vs. RHE for a pH of 13.6. Such a shift was found to be robust against the use of different definitions of V_{onset}. We used as control the method introduced by Butler,[35] in which J^2 is plotted against V and the apparent flatband potential in hematite is determined as the potential at which the extrapolation of the linear relationship between J^2 and V intercepts with $J^2 = 0$. Since this model only deals with the properties of the semiconductor and not with those of the semiconductor/electrolyte interface, a correspondence can be established between V_{onset} and the sum of V_{fb} and all of the overpotentials required to start the OER. Using this method, we obtained values of V_{onset} of 1.6 and 1.28 vs. RHE for pH of 6.9 and 13.6 respectively, as shown in the Supporting Information, Figure S7. Thus, the same shift of V_{onset} of 320 mV was obtained. The shift of V_{onset} with increasing pH towards more cathodic potentials follows a linear trend, as shown by the fit of the data resulting in a linear coefficient of 49 mV per pH unit. This is in good agreement with calculations of the relative stability between the OH- and O-terminated surfaces.

Further discussion is required to rule out that the observed cathodic shift in V_{onset} is due to variation of other

properties in the system when increasing the pH. First, the flatband potential V_{fb} was obtained by extrapolation of the linear part of Mott–Schottky (MS) plots, which were recorded with electrolytes of pH equal to 6.9, 11 and 13.6. As shown in the Supporting Information, Figure S8b, V_{fb} is found to be 0.65 V versus RHE irrespective of the pH. Second, open circuit measurements were performed in dark and under illumination, and the difference between open circuit potential in the former and the latter case was taken in order to determine the photovoltage V_{ph} of the hematite film. V_{ph} was found to be about 0.23 V for all electrolytes tested. Such a photovoltage is in very good agreement with previous reports on bare hematite films.[36] Finally, it is also possible to rule out the possibility that the shift of V_{onset} is caused by an increase in the conductivity of the electrolyte, owing to the following argument. The uncompensated resistance of the electrolyte, R_u, was measured for all electrolytes prior to the cyclic voltammetry experiments and found to be between 130 Ω and 135 Ω, with the two extremes for pH 6.9 and pH 13.6 respectively. The highest difference in the uncompensated potential drop owing to the resistance of the electrolyte can then be estimated to be 0.375 mV, which is negligible.

Finally, it is worth commenting on the electrochemical properties of the system without illumination, that is, on the OER in the dark. Previous electrochemical studies have shown that the required potential for the OER to become thermodynamically favorable is about 1.7 V, independent of the pH.[9,10] The dark OER current was measured, and the resulting *J*–*V* curves are plotted in the Supporting Information, Figure S10. If the onset potential is defined in the same way as previously done for the photocurrent, the total shift of V_{onset} upon varying the pH from 6.9 to 13.6 is 46 mV, which is considerably smaller than the 320 mV shift of V_{onset} under illumination.

In conclusion, we investigated, both theoretically and experimentally, the role of surface states on the OER on hematite. DFT-based calculations revealed that the DOS of both the OH-terminated and O-terminated hematite surfaces contains surface states, however with a different spectral distribution. At low applied potentials, the surface states act as recombination center for holes on the OH-terminated surface. At higher potentials, the O-terminated surface becomes more stable and the OER takes place by surface states with energy close to the top of the valence band. Finally, for yet more anodic potentials, the OER proceeds via direct transfer of holes from the valence band. The calculations also predicted that the relative stability between the OH- and O-terminated surfaces follows a Nernstian dependence on the pH. We demonstrated a cathodic shift of V_{onset} for the OER under illumination upon increasing the pH from 6.9 to 13.6, while the maximum photocurrent showed no dependence on the pH. The observed shift follows a linear trend with a coefficient of 49 mV per pH unit, in good agreement with the predicted Nernstian behavior. Detailed PEC characterization indicated that the energy levels of the surface states through which the OER takes place at moderately high bias shift in very good agreement with the magnitude of V_{onset}. Moreover, open-circuit voltage measurements indicated that the photovoltage of hematite is independent of the pH. These findings are significant as they contribute to elucidate the role played by surface states in the photon induced OER on hematite, which had remained elusive thus far. More generically, the results presented lead to a deeper understanding of the PEC properties of hematite, which is required to fully exploit the potential of this earth-abundant, promising semiconductor for water splitting.

Experimental Section

DFT calculations were based on theory as implemented in VASP. The Kohn–Sham orbitals were expanded using plane waves with a kinetic energy cutoff of 450 eV. The projector augmented wave method was used to describe the interaction between valence electrons and the core.[37,38] Six valence electrons for each O atom ($2s^2 2p^4$) and eight valence electrons for each Fe atom ($3d^7 4s^1$) were taken into account. The xc-functional was approximated by the spin-polarized Perdew–Burke–Ernzerhof (PBE) formula.[39] Owing to the strong electron correlation in 3d metal oxides, the + U method was used. Values for U and J were fixed to 4.3 and 1, in accordance with Carter et al.[10] The hematite was modeled in its hexagonal cell and the surface slabs used four complete (Fe-O3-Fe) units. The structures were relaxed until the forces were less than 0.01 eV Å^{-1}. In the computational electrochemical framework used here, the energy of the $H^+ + e^-$ pair is related to that of $1/2\,H_2$ in the gas-phase by the relative hydrogen electrode (RHE) at electrochemical potential $V = 0$, and the applied electrochemical potential V shifts the stability of all deprotonation steps by an amount equal to eV.

Hematite thin films were fabricated on top of indium tin oxide (ITO) coated glass substrate according to a procedure described in previous work.[28] All the PEC characterization (cyclic voltammetry, open circuit potential measurements, EIS and MS characterization) were performed in a standard three-electrode configuration with the hematite film as working electrode, a Pt wire as counter-electrode, and a Ag/AgCl electrode as reference. Electrolytes with pH ranging from 6.9 to 13.6 were prepared from 0.5 M Na_2SO_4 solutions in MilliQ water by addition of an appropriate amount of KOH. Magnetic stirring was applied to the PEC during all the cyclic voltammetry measurements. The potential was converted from the Ag/AgCl scale to the RHE scale using the Nernst equation. The surface of the working electrode typically exposed to the electrolyte was around 0.3 cm^2. EIS was performed under illumination by applying a superposition of DC and AC voltage. The latter had amplitude of 10 mV and frequency ranging between 10^5 and 0.1 Hz. MS analysis was carried out in the dark at a frequency of 10^4 Hz. Further details on fabrication and physical and PEC characterization can be found in the Supporting Information.

Received: July 2, 2014
Revised: August 25, 2014
Published online: October 3, 2014

Keywords: energy conversion · hematite · photoelectrochemistry · surface states · water splitting

[1] M. Grätzel, *Nature* **2001**, *414*, 338.
[2] Y. Tachibana, L. Vayssieres, J. R. Durrant, *Nat. Photonics* **2012**, *6*, 511.
[3] M. G. Walter, E. L. Warren, J. R. McKone, S. W. Boettcher, Q. Mi, E. A. Santori, N. S. Lewis, *Chem. Rev.* **2010**, *110*, 6446.
[4] T. Bak, J. Nowotny, M. Rekas, C.. Sorrell, *Int. J. Hydrogen Energy* **2002**, *27*, 991.
[5] F. E. Osterloh, *Chem. Mater.* **2008**, *20*, 35.

[6] K. L. Hardee, *J. Electrochem. Soc.* **1976**, *123*, 1024.
[7] N. Beermann, L. Vayssieres, S.-E. Lindquist, A. Hagfeldt, *J. Electrochem. Soc.* **2000**, *147*, 2456.
[8] A. Kay, I. Cesar, M. Grätzel, *J. Am. Chem. Soc.* **2006**, *128*, 15714.
[9] A. Hellman, R. G. S. Pala, *J. Phys. Chem. C* **2011**, *115*, 12901.
[10] P. Liao, M. C. Toroker, E. A. Carter, *Nano Lett.* **2011**, *11*, 1775.
[11] Y. Lin, S. Zhou, S. W. Sheehan, D. Wang, *J. Am. Chem. Soc.* **2011**, *133*, 2398.
[12] J. Brillet, J.-H. Yum, M. Cornuz, T. Hisatomi, R. Solarska, J. Augustynski, M. Grätzel, K. Sivula, *Nat. Photonics* **2012**, *6*, 824.
[13] H. Dotan, O. Kfir, E. Sharlin, O. Blank, M. Gross, I. Dumchin, G. Ankonina, A. Rothschild, *Nat. Mater.* **2013**, *12*, 158.
[14] S. C. Warren, K. Voïtchovsky, H. Dotan, C. M. Leroy, M. Cornuz, F. Stellacci, C. Hébert, A. Rothschild, M. Grätzel, *Nat. Mater.* **2013**, *12*, 842.
[15] L.-S. R. Yeh, *J. Electrochem. Soc.* **1977**, *124*, 833.
[16] T. W. Hamann, *Dalton Trans.* **2012**, *41*, 7830.
[17] P. Liao, J. A. Keith, E. A. Carter, *J. Am. Chem. Soc.* **2012**, *134*, 13296.
[18] K. M. H. Young, B. M. Klahr, O. Zandi, T. W. Hamann, *Catal. Sci. Technol.* **2013**, *3*, 1660.
[19] *Photoelectrochemical Hydrogen Production* (Eds.: R. van de Krol, M. Grätzel), Springer, Boston, MA, **2012**.
[20] B. Klahr, S. Gimenez, F. Fabregat-Santiago, T. Hamann, J. Bisquert, *J. Am. Chem. Soc.* **2012**, *134*, 4294.
[21] G. Kresse, J. Hafner, *Phys. Rev. B* **1993**, *47*, 558.
[22] G. Kresse, J. Hafner, *Phys. Rev. B* **1994**, *49*, 14251.
[23] G. Kresse, *Phys. Rev. B* **1996**, *54*, 11169.
[24] J. Rossmeisl, Z.-W. Qu, H. Zhu, G.-J. Kroes, J. K. Nørskov, *J. Electroanal. Chem.* **2007**, *607*, 83.
[25] J. Nørskov, T. Bligaard, A. Logadottir, S. Bahn, L. B. Hansen, M. Bollinger, H. Bengaard, B. Hammer, Z. Sljivancanin, M. Mavrikakis, Y. Xu, S. Dahl, C. J. H. Jacobsen, *J. Catal.* **2002**, *209*, 275.
[26] G. Rollmann, A. Rohrbach, P. Entel, J. Hafner, *Phys. Rev. B* **2004**, *69*, 165107.
[27] T. P. Trainor, A. M. Chaka, P. J. Eng, M. Newville, G. A. Waychunas, J. G. Catalano, G. E. Brown, *Surf. Sci.* **2004**, *573*, 204.
[28] B. Iandolo, M. Zäch, *Aust. J. Chem.* **2012**, *65*, 633.
[29] J. Bisquert, *Phys. Chem. Chem. Phys.* **2008**, *10*, 49.
[30] B. Klahr, S. Gimenez, F. Fabregat-Santiago, J. Bisquert, T. W. Hamann, *Energy Environ. Sci.* **2012**, *5*, 7626.
[31] L. M. Peter, K. G. U. Wijayantha, A. A. Tahir, *Faraday Discuss.* **2012**, *155*, 309.
[32] L. Badia-Bou, E. Mas-Marza, P. Rodenas, E. M. Barea, F. Fabregat-Santiago, S. Gimenez, E. Peris, J. Bisquert, *J. Phys. Chem. C* **2013**, *117*, 3826.
[33] F. Le Formal, N. Tétreault, M. Cornuz, T. Moehl, M. Grätzel, K. Sivula, *Chem. Sci.* **2011**, *2*, 737.
[34] F. Le Formal, M. Grätzel, K. Sivula, *Adv. Funct. Mater.* **2010**, *20*, 1099.
[35] M. A. Butler, *J. Appl. Phys.* **1977**, *48*, 1914.
[36] C. Du, X. Yang, M. T. Mayer, H. Hoyt, J. Xie, G. McMahon, G. Bischoping, D. Wang, *Angew. Chem. Int. Ed.* **2013**, *52*, 12692; *Angew. Chem.* **2013**, *125*, 12924.
[37] P. E. Blöchl, *Phys. Rev. B* **1994**, *50*, 17953.
[38] G. Kresse, D. Joubert, *Phys. Rev. B* **1999**, *59*, 1758.
[39] J. P. Perdew, K. Burke, M. Ernzerhof, *Phys. Rev. Lett.* **1997**, *78*, 1396.